RESEARCH ARTICLE | FEBRUARY 06 2026

Does correlated orbital theory improve PBE-like functionals?

Rodrigo A. Mendes ; Zachary W. Windom ; Roberto L. A. Haiduke ; Rodney J. Bartlett

J. Chem. Phys. 164, 054113 (2026)
https://doi.org/10.1063/5.0298139

The Journal of Chemical Physics ARTICLE pubs.aip.org/aip/jcp

Does correlated orbital theory improve PBE-like functionals?

Cite as: J. Chem. Phys. 164, 054113 (2026); doi: 10.1063/5.0298139
Submitted: 22 August 2025 • Accepted: 19 January 2026 •
Published Online: 6 February 2026

Rodrigo A. Mendes,[1] Zachary W. Windom,[1] Roberto L. A. Haiduke,[2,a)] and Rodney J. Bartlett[1,a)]

AFFILIATIONS

[1] Quantum Theory Project, University of Florida, Gainesville, Florida 32611, USA
[2] São Carlos Institute of Chemistry, University of São Paulo, 13566-590 São Carlos, SP, Brazil

[a)] **Authors to whom correspondence should be addressed:** haiduke@iqsc.usp.br and bartlett@qtp.ufl.edu

ABSTRACT

Correlated Orbital Theory (COT) provides an exact one-particle framework by imposing rigorous physical constraints on Kohn–Sham eigenvalues and, as a consequence, directly incorporates essential electron correlation into molecular orbitals. This approach paves the way toward a new class of approximations within Kohn–Sham Density Functional Theory (KS-DFT). However, since all existing quantum theory project functionals are derived from CAM-B3LYP, we pose the question: Can COT improve the hybrid versions of different exchange-correlation functionals as well? To that end, we explore two optimization strategies for adjusting the existing parameters within PBE0, TPSS0, and LC-PBE0: (*i*) the ionization potential condition and (*ii*) the HOMO–LUMO condition. In this sense, we critically assess how these functionals address the "Devil's Triangle" of KS-DFT: self-interaction error, integer discontinuity, and one-particle spectra. We further examine how the COT influences the description of two challenging properties, charge transfer and reaction barrier heights. Overall, enforcing both COT conditions systematically enhances the performance of functionals within the PBE family, although the description of reaction barriers still leaves room for improvement.

I. INTRODUCTION

At present, the most widely used method in electronic structure investigations is certainly Kohn–Sham (KS) Density Functional Theory (DFT).[1,2] In KS-DFT, the only unknown component is the exchange-correlation (XC) functional, which has led to the development of numerous expressions over the years. One of the most successful XC functionals is the one proposed by Perdew–Burke–Ernzerhof (PBE).[3] PBE belongs to the class of Generalized Gradient Approximation (GGA) functionals. These so-called semi-local functionals depend on both the electron density (ρ) and its gradient ($\nabla\rho$) and, generally, are represented by

$$E_{xc}^{GGA} = \int \varepsilon_{xc}^{GGA}(\rho, \nabla\rho)\rho(\vec{r})d\vec{r}. \tag{1}$$

Following the Jacob's ladder concept for XC functionals,[4] the design philosophy behind PBE was extended to the development of the Perdew–Kurth–Zupan–Blaha (PKZB) functional,[5] a meta-GGA (MGGA) family member. MGGA functionals go beyond the GGA idea by incorporating additional ingredients such as the Laplacian of the electron density ($\nabla^2\rho$) or the kinetic energy density of the occupied Kohn–Sham orbitals (τ). In this sense, the PKZB functional was subsequently refined, leading to the development of the Tao–Perdew–Staroverov–Scuseria (TPSS) functional.[6] Anyway, these functionals share the same general form

$$E_{xc}^{MGGA} = \int \varepsilon_{xc}^{MGGA}(\rho, \nabla\rho, \tau)\rho(\vec{r})d\vec{r}, \tag{2}$$

where $\tau(\vec{r}) = \frac{1}{2}\sum_i^{occ} |\nabla\phi_i(\vec{r})|^2$.

Despite numerous advances, KS-DFT remains inherently limited by persistent deficiencies; namely, the self-interaction error (SIE), the lack of derivative discontinuity, and an inaccurate one-electron energy spectrum, all of which are interrelated but, from a developmental viewpoint, offer three different routes for improvement.

A pivotal step toward mitigating these issues was achieved by incorporating the non-local Hartree–Fock (HF) exchange potential (v_x^{HF}) into the KS-DFT world. Consequently, the conventional approach involves adding a fraction of HF exchange within a given

exchange functional from DFT, resulting in what are known as hybrid functionals. For certain properties, such as excitation energies, hybrid functionals can achieve even greater accuracy when the exchange operator (v_x^{hybrid}) is partitioned into short- and long-range components, $E_x = E_x^{SR} + E_x^{LR}$. Such a class of functionals is known as range-separated hybrid (RSH).[7–9] In this framework, the Coulomb operator (r_{12}^{-1}) is generalized as

$$\frac{1}{|r_1 - r_2|} = \underbrace{\frac{1 - erf(\mu|r_1 - r_2|)}{|r_1 - r_2|}}_{\text{short-range}} + \underbrace{\frac{erf(\mu|r_1 - r_2|)}{|r_1 - r_2|}}_{\text{long-range}}, \tag{3}$$

where *erf* is the error function and μ is the range-separation parameter. This long-range correction (LC) approach enables a more balanced treatment of electron interactions over different distances. For instance, LC-PBE0[10] is the RSH version of PBE0,[11] retaining 25% of v_x^{HF} plus 75% of PBE exchange (v_x^{PBE}) at short-range (as in PBE0), while employing 100% of HF exchange in the long-range regime. The following energy expression represents, in general, the LC exchange functionals,

$$E_x^{LC} = \alpha E_x^{SR-HF} + (1 - \alpha) E_x^{SR-DFT} + (\alpha + \beta) E_x^{LR-HF}, \tag{4}$$

where two additional parameters, α and β, are introduced. The former determines the appropriate admixture of HF and DFT exchange at short range, while their sum defines the amount of HF exchange at the long-range limit. Over the years, various RSH functionals based on PBE have been proposed, with or without modifications to the PBE exchange (e.g., LC-ωPBE,[12] LRC-ωPBEH,[13] CAM-PBEH,[14] and tuned LC-PBE,[15] among others). These functionals differ in the fraction of HF exchange and the range-separation parameter, and they show better performance for ionization potential/electron affinity spectra and excitation energies.[16,17]

Although global hybrid XC functionals generally outperform their pure GGA or MGGA counterparts, they are still significantly affected by SIE.[18,19] Moreover, global hybrids fail to reproduce the correct behavior associated with the integer discontinuity,[20] also performing poorly in the simulation of one-electron spectra.[21,22]

In this context, the exchange-correlation functionals developed by us, the Quantum Theory Project (QTP), represent a decisive step toward solving these issues. Therefore, QTP functionals follow the Correlated Orbital Theory (COT),[23] which incorporates rigorous physical constraints on Kohn–Sham eigenvalues by tying observable quantities such as vertical ionization potentials (IPs) and electron affinities (EAs) to the negative of occupied ($-\varepsilon_i$) and some unoccupied orbitals ($-\varepsilon_a$), respectively. COT not only corrects important spectral deficiencies but also provides a path for achieving a new class of KS-DFT approximations that inherit the interpretive clarity and high-level accuracy of wave function-based methods while maintaining the computational tractability of KS-DFT. Although several other approaches have been proposed to mitigate delocalization and self-interaction errors (e.g., PZ-SIC,[24] LOSC,[25] and FLOSIC,[26] among others), COT stands apart as an independent framework, or even a philosophy, for developing XC functionals in which these issues are naturally corrected.

All RSH functionals from the QTP family, QTP00,[27] QTP01,[28] QTP02,[29] and LC-QTP,[29] are derived from CAM-B3LYP;[30] while QTP17[31] is similar to B3LYP.[32–35] These functionals have demonstrated success in accurately describing a wide range of ground-state properties, e.g., ionization potentials,[21,36] electron affinities,[22] isotropic hyperfine coupling constants,[37] and reaction barrier heights.[29] In addition, they perform very well for various response properties, such as core excitation energies,[38] vertical excitation energies (Rydberg and charge-transfer states),[17] two-photon absorption cross sections,[39] and a variety of second-order response properties (including static polarizability, J-coupling, and chemical shift).[40] Notably, QTP functionals have also demonstrated CC/EOM-CC quality in predicting both the fundamental and optical gaps of challenging extended systems, such as polyacene and *trans*-polyacetylene oligomers,[41] although they will still suffer from having 100% HF exchange in long-range for infinite systems.[42]

Given the demonstrated success of QTP functionals, a natural question arises: Can COT improve the hybrid versions of XC functionals from different families as well? To address this point, we selected three PBE-based functionals from different rungs of Jacob's ladder: (1) PBE0, a hybrid GGA; (2) TPSS0, a hybrid MGGA; and (3) LC-PBE0, a range-separated hybrid functional. Therefore, to evaluate the potential improvements introduced by COT, two reparameterization strategies are considered here for adjusting the admixture of HF and PBE-like exchange.

In the first approach, we enforced the exact COT condition that the negative of all occupied Kohn–Sham orbital energies should correspond to IPs (with or without the core electrons). We refer to this proposal as the IP condition. In the second approach, along with the IP condition for the highest occupied molecular orbital (HOMO) and by insisting that the negative of the energy of the lowest unoccupied molecular orbital (LUMO) corresponds to the EA, we enforced the HOMO–LUMO COT condition. The HOMO–LUMO condition is an obvious partial fix for any integer discontinuity problem! The EA is equivalent to an IP via the HOMO/LUMO condition. Therefore, in this case, only the first IP and EA values are considered, which are here referred to as the HOMO/LUMO condition (although the full spectrum can be examined). Further details on both approaches are provided in Sec. III.

II. THEORY

The modification of the Dyson equation from Electron Propagator (EP) theory by coupled-cluster (CC)[43] leads to an exact one-particle correlated orbital theory,[23] which serves as the foundation for the development of the QTP functionals. The Dyson/EP theory provides quasiparticle energies and orbitals by solving the corresponding eigenvalue equation

$$[\hat{f} + \hat{\Sigma}(\omega)]\psi_p(\omega) = \varepsilon_p \psi_p(\omega), \tag{5}$$

where the frequency-dependent self-energy $\hat{\Sigma}(\omega)$ introduces correlation corrections on top of the single-particle Fock operator, $\hat{f} = \hat{t} + \hat{v} + \hat{J} - \hat{K} = \hat{h} + \hat{J} - \hat{K}$. Here, $\hat{t}$, $\hat{v}$, $\hat{J}$, and $\hat{K}$ are the usual kinetic energy, electron–nucleus interaction, electron–electron Coulomb, and exchange operators.

The eigenvalues of this equation arise when the frequency on the left-hand side matches that on the right-hand side. A major advantage of CC theory is that by inserting a CC ground-state

wave function into the EP theory, the frequency dependence of the self-energy is eliminated, yielding the COT equation

$$[\hat{f} + \hat{\Sigma}_{CC}]\psi_p = \varepsilon_p \psi_p, \tag{6}$$

where $\hat{\Sigma}_{CC}$ is the frequency-independent self-energy operator. Its bi-orthogonal orbital solutions and eigenvalues define a one-particle, correlated orbital theory.

The next step is to recognize that the COT equation is now numerically equivalent to the solutions of the IP/EA-EOM-CC method,[43–45]

$$\bar{H}R_k = \omega_k R_k, \tag{7}$$

where R_k is the amplitude for the kth right-hand state. A subset of these eigenvalues corresponds, for example, to the "principal" IPs. In the IP case at CCSD, R_k consists of 1-hole (1h), 2-holes (2h), and 1-particle (1p) operators, and $\omega_k = (I_j)$ for j occupied IPs. In the EA case, R_k consists of 1p, 2p, and 1h operators, and $\omega_k = (A_b)$ for the b primary electron affinities. The EOM-CC solutions are now expressed in configuration space, instead of the one-particle space of the Dyson equation that, from a different viewpoint, would correspond to a Löwdin partitioning of the exact equations, instead of the frequency-independent partitioning emphasized in our COT paper.[23] However, the fundamental element remains the justified removal of the frequency dependence from the Dyson equation that puts these CC inspired COT equations into the same computational domain as HF or KS theory. It also decouples the IP and EA parts of the one-body Greens' function, greatly simplifying its solution in an infinite-order frequency-independent form. Its removal is also useful to the GW procedure, as the integration over the frequency is the rate-determining step in the calculation. Another particularly useful by-product of COT is that the initial solutions of the IP/EA-EOM-CC equations are the 'principal' ones, relegating the other shake-up, etc., solutions to higher order, where one should add additional particle–hole operators for accurate descriptions.

In this sense, by construction, the correlated orbital theory imposes the following conditions on top of single-particle wave function theories:

$$IP_i = -\varepsilon_i = -\langle \phi_i \mid \hat{h}_i + \hat{J} - \hat{K} + \hat{\Sigma}_{CC} \mid \phi_i \rangle, \tag{8}$$

and

$$EA_a = -\varepsilon_a = -\langle \phi_a \mid \hat{h}_a + \hat{J} - \hat{K} + \hat{\Sigma}_{CC} \mid \phi_a \rangle, \tag{9}$$

where ϕ_i and ϕ_a represent, respectively, the occupied and unoccupied orbitals.

In the Kohn–Sham framework, the term $\hat{J} - \hat{K} + \hat{\Sigma}_{CC}$ is replaced by $\hat{J} + \hat{v}_{xc}$, where v_{xc} is the exchange-correlation potential. Accordingly, Eq. (8) can be approximated as

$$IP_i \approx -\varepsilon_i = -\langle \phi_i \mid \hat{h}_i + \hat{J} + \hat{v}_{xc} \mid \phi_i \rangle, \tag{10}$$

with a similar expression applied to Eq. (9). This condition should be viewed as a constraint on KS-DFT, as the accuracy of $\hat{v}_{xc}$ is tested by this IP eigenvalue condition. As discussed elsewhere,[19] this is also critical to how well a KS-DFT approximation satisfies correct self-interaction.

Because Bartlett's IP-eigenvalue theorem (KS-DFT's Koopmans' theorem) is rigorously satisfied by Dyson theory and its CC modification, any KS-DFT should be required to satisfy this as a prerequisite to making KS-DFT provide accurate results. That is what the QTP functionals attempt to do.

Further consequences follow. COT enables the following relationships for vertical processes of electron loss or gain:

$$IP_i(M) = -\varepsilon_i(M) = EA_a(M^+) = -\varepsilon_a(M^+), \tag{11}$$

and

$$EA_a(M) = -\varepsilon_a(M) = IP_i(M^-) = -\varepsilon_i(M^-). \tag{12}$$

Here, M, M^+, and M^- refer to the neutral, cationic, and anionic states of a molecular system, respectively. Hence, in Eq. (11), i labels the occupied orbital of M involved in the electron removal process for achieving M^+, while a refers to the virtual orbital of M^+ that must be filled by an electron to recover M. Analogous interpretations hold for Eq. (12), but considering now M and M^-. Therefore, if the COT conditions are exactly satisfied, the differences in the eigenvalues for the orbitals presented in Eqs. (11) and (12) should ideally vanish.

III. COMPUTATIONAL METHODS

The DFT calculations were performed within NWChem 7.0.2,[46] unless otherwise stated. The basis set chosen for the reparameterization process was aug-cc-pVQZ.[47,48] The new XC functionals are developed based on arguments from COT,[23] and two different procedures are employed along this reparameterization process: (*i*) IP condition and (*ii*) HOMO–LUMO condition. In addition, the following basis sets were used throughout the paper: cc-pVDZ[47](charge-transfer), cc-pVTZ[47] (vertical IPs), aug-cc-pVTZ[47,48] (H_2^+ potential curve, fractional occupation of H_2O/OH, and vertical EAs), jul-cc-pV(T+d)Z[49] (long-range charge-transfer), and def2-QZVP[50] (barrier heights). Information regarding the molecular geometries of all systems used within this study is provided in the supplementary material.

A. IP condition

This procedure relies on the central argument from COT that the negative of the eigenvalues obtained for occupied orbitals should provide the corresponding exact ionization potentials. This approach was previously followed in the development of QTP00[27] and QTP17,[31] which fitted the parameters in order to reproduce all five experimental IPs of water. It is noteworthy that the specific choice of molecule is not particularly important in COT. Water was selected simply because its IPs are well-established experimentally; it could just as well have been any other molecule. Naturally, different molecules would lead to different parameters; however, we expect an approximate universality of the IP when the method is tested across a broader set of systems. That is, using parameters optimized for water, we obtain equally good agreement with the observed IPs of 42 arbitrarily chosen molecules, suggesting that any one of them could have served just as well as water in determining the parameters.[51]

In the present study, we adopted the same strategy for LC-PBE0, fitting its parameters to match the same five IP values of water. However, we restricted the fitting procedure to the four valence IPs of water for PBE0 and TPSS0, that is, excluding the core O(1s)

result, since it was not possible to adjust parameter values that simultaneously yield accurate results across all orbitals for these global hybrids. To this end, the performance of PBE0, TPSS0, and LC-PBE0 was investigated, searching for new parameterizations of analogous functionals using the same generalized gradient or meta-generalized gradient approximation components, specifically, PBE/TPSS for both exchange (X) and correlation (C).[3,5,52] The results were evaluated using the mean absolute deviation (MAD), although maximum absolute deviation (MAX) values are also reported. All information regarding the valence IP values of water can be seen in the supplementary material.

B. HOMO/LUMO condition

This procedure follows the relations introduced in Eqs. (11) and (12), which explore COT in a broader aspect. Hence, in addition to the initially imposed IP condition for the HOMO, the EA conditions anticipated by COT are also taken into consideration. This means that no experimental values were used to optimize the parameters of these functionals. Therefore, during the conception of QTP02 and LC-QTP, Haiduke and Bartlett[29] proposed rewriting Eqs. (11) and (12) using H_2O, the OH radical, and their ions, that is,

$$IP(H_2O) = -\varepsilon_{HOMO}(H_2O) = EA(H_2O^+) = -\varepsilon_{LUMO}(H_2O^+), \quad (13)$$

and

$$EA(OH) = -\varepsilon_{LUMO}(OH) = IP(OH^-) = -\varepsilon_{HOMO}(OH^-). \quad (14)$$

Therefore, the optimum parameters are chosen as the ones providing similar values for both of the following absolute energy differences:

$$\Delta\varepsilon_1 = |\, \varepsilon_{HOMO}(H_2O) - \varepsilon_{LUMO}(H_2O^+)\,|, \quad (15)$$

and

$$\Delta\varepsilon_2 = |\, \varepsilon_{LUMO}(OH) - \varepsilon_{HOMO}(OH^-)\,|, \quad (16)$$

which should be ideally zero in COT.

Specifically for the LC-PBE0 case, different sets of μ and α (β) were identified as minimizing Eqs. (15) and (16). Following an approach similar to that of Haiduke and Bartlett, we employed additional relationships using two different transition metal systems (CuH and ZnF) and their corresponding ions. The adapted forms of Eqs. (13)–(16) are provided in the supplementary material (Eqs. S5–S8).

In other words, the parameterization of existing functionals can be performed to accurately satisfy one of these two relations, providing almost negligible values for $\Delta\varepsilon_1$ or $\Delta\varepsilon_2$. However, it seems not possible to exactly satisfy both relations at the same time with the XC functionals available at present, and the procedure chosen here tries to achieve a more balanced description of both electron loss and electron gain processes.

At this point, it is also evident that the HOMO/LUMO condition can be viewed as an "integer discontinuity condition," since it considers the addition or removal of electrons to/from the neutral system. In more detail, these conditions imply that the slopes of the lines achieved by varying the number of electrons between a neutral system and its cation, as well as between a neutral system and its anion, should be as similar as possible in the neighborhood of the associated systems with an integer number of electrons. In other words, the linearity behavior expected from the exact XC functional by varying the number of electrons during electron gain or electron removal processes, as predicted by Perdew and co-workers,[53] is enforced by the exact HOMO/LUMO conditions.

IV. RESULTS

As mentioned before, H_2O was selected as the reference system for the reparametrization procedure based on the IP condition, while the set of systems used for HOMO/LUMO condition optimization includes neutral, cationic, and anionic forms of H_2O/OH molecules. This choice reflects an established precedent, as these molecules have been used in the development of QTP00–QTP02 functionals.[27–29] Table I presents the values achieved for the optimum percentage of Hartree–Fock exchange starting from PBE0 and TPSS0.

As can be seen, similar to the situation observed with the regular version of these functionals, the reparameterization based on the IP condition results in a similar amount of HF exchange for both PBE0 and TPSS0, 71%. Therefore, considering the four valence IPs of H_2O, the PBE IP shows a mean absolute deviation (MAD) of 0.50 eV relative to experimental values. Similarly, TPSS0 IP provides a MAD of 0.51 eV. This procedure clearly seems to favor larger amounts of HF exchange (up to 71%). All values are depicted in the supplementary material.

Next, concerning the HOMO–LUMO condition for the reparameterization step, the HF exchange percentages now decrease relative to those found with the IP condition, although the values are still large. For example, PBE0 HL contains 66% of HF exchange, while TPSS0 HL presents 65%, again providing similar amounts of HF exchange. Therefore, $\Delta\varepsilon_1 \approx \Delta\varepsilon_2 \approx 0.46$ eV in the case of PBE0 HL and ≈0.44 eV for TPSS0 HL. Therefore, this procedure also tends to result in a larger amount of HF exchange compared to the original versions of these PBE-based global hybrids.

Table II presents the optimal range-separation parameters (α, β, and μ) for LC-PBE0 and for the versions of this functional proposed in this study. In this case, similarly to the regular LC-PBE0, the exact $\alpha + \beta = 1$ condition was also imposed during the reparameterization, thereby reducing the number of independent parameters. This condition also means that all versions of this functional consider 100% of HF exchange at the long-range limit. For most spectroscopic applications, this long-range corrected form seems excellent, but as mentioned earlier, it is not ideal for solid-state applications. Therefore, from the IP condition procedure, considering all five experimental ionization potentials of H_2O, the optimal LC-PBE0 IP parameter set yielded a MAD of 0.26 eV. For the parameters selected based on the HOMO/LUMO condition, the errors defined in Eqs. (15) and (16) were 0.74 and 0.71 eV, respectively. In

TABLE I. Percentage of HF exchange in PBE0, TPSS0, and in the new versions of these functionals proposed here.

XC	Regular (%)	IP (%)	HL (%)
PBE0	25	71	66
TPSS0	25	71	65

TABLE II. Range separation parameters in LC-PBE0 and the new versions of this functional proposed here.

XC	α	β	μ
Regular	0.25	0.75	0.30
IP	0.57	0.43	0.18
HL	0.34	0.66	0.28

addition, the IP condition procedure still favors larger amounts of HF exchange at short-range than the HOMO–LUMO condition, 57% and 34%, respectively.

A. Self-interaction error

We first investigate the ability of the functionals in reproducing the potential energy curve (PEC) of H_2^+. As illustrated in Fig. 1, the correct dissociation limit is exactly satisfied by the Unrestricted Hartree–Fock (UHF) method. In this case, SIE, which is universally present in DFT, tends to negatively affect the energy results as any XC functional is chosen for this task. For example, some functionals shown in Fig. 1 significantly underestimate the energies in the dissociation limit region. The functionals exhibiting this behavior more dramatically include regular PBE0 and TPSS0 (solid red and blue lines).

Interestingly, reparameterizations following the IP and HL conditions from COT considerably mitigate the SIE of PBE0 and TPSS0, as shown by the red and blue dashed/dotted lines in Fig. 1. Although these functionals still exhibit some degree of SIE, the deviations compared to the UHF curve are now much smaller than those of the regular versions of these functionals. For example, at 10 Å, the deviations of the PBE0-based functionals compared to UHF are −43.86 kcal/mol (regular PBE0), −18.04 kcal/mol (PBE0 IP), and −20.78 kcal/mol (PBE0 HL). For TPSS0-type functionals, the deviations are −41.21 kcal/mol (regular), −15.52 kcal/mol (TPSS0 IP), and −18.80 kcal/mol (TPSS0 HL).

On the other hand, all versions of LC-PBE0 exhibit better behavior considering the PEC of H_2^+. According to Cohen *et al.*,[54] this behavior is expected; that is, these authors observed that the only class of XC functionals that showed some improvement relative to SIE was the one containing range separation in the exchange operator. Again, both the IP and HL versions of LC-PBE0 perform slightly better than the regular version of this XC functional. In these cases, the deviations with respect to UHF at 10 Å are −14.09 kcal/mol (regular LC-PBE0), −13.40 kcal/mol (LC-PBE0 IP), and −13.50 kcal/mol (LC-PBE0 HL).

B. Integer discontinuity

Another fundamental issue in DFT is the so-called integer discontinuity, which arises when electrons are added to or removed from a chemical system. The expected behavior from the exact XC functional would be that of a linear total energy variation with the number of electrons between the associated systems with integer values, that is, providing a straight line connecting the energies of the systems with N_0, $N_0 + 1$, and $N_0 - 1$ electrons. Figure 2 shows the results of calculations that consider the removal or addition of fractional electron occupations, up to the complete ionization or electron attachment of/to H_2O and OH, respectively.

We evaluate the PBE-like functionals against the "exact" behavior, represented by a linear interpolation between the experimental ionization potential of H_2O and the electron affinity of OH, as illustrated by the black line in Fig. 2. In this sense, we observe that

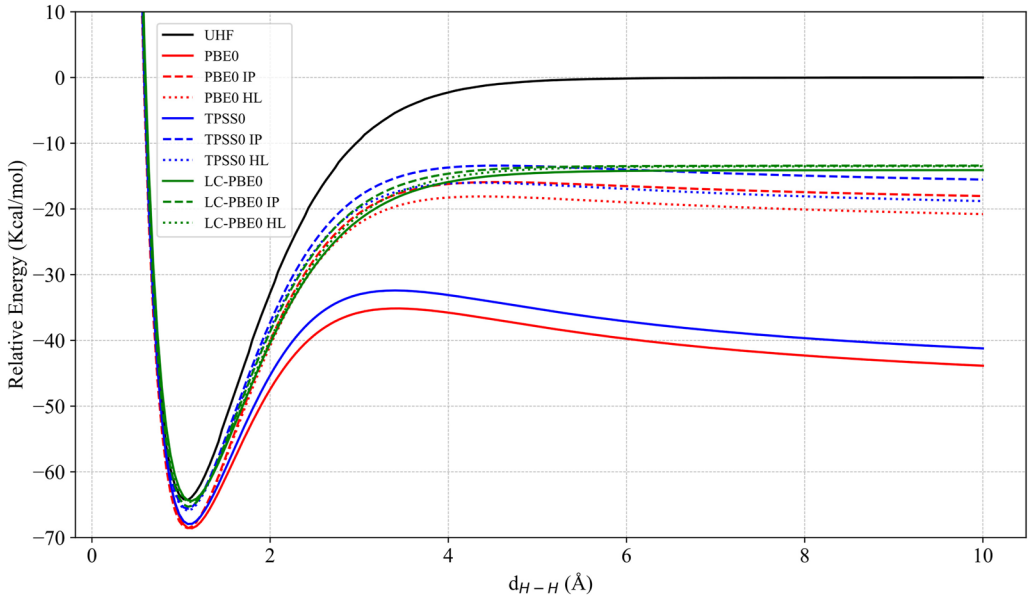

FIG. 1. Potential energy curves of H_2^+ with respect to the exact dissociation limit energy (−0.50 a.u.) against internuclear distances (d_{H-H}) obtained with PBE-like exchange-correlation functionals.

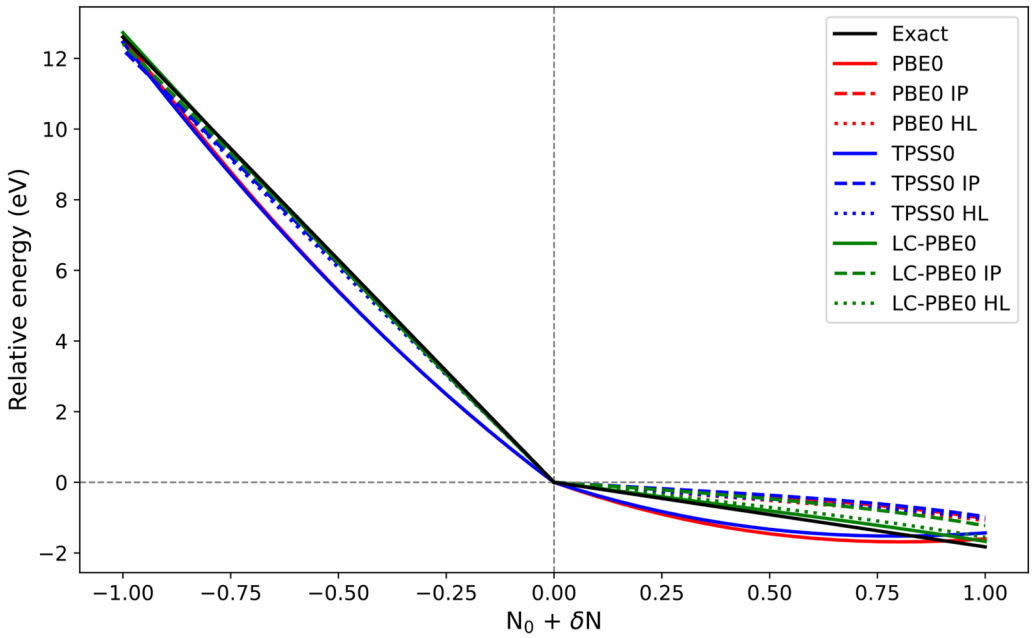

FIG. 2. Relative energy for water (left) and hydroxyl (right) calculations for systems with fractional occupation numbers (ONs). In this case, ON = 0.0 represents H_2O and OH, while ON values of −1.0 and 1.0 are associated, respectively, with H_2O^+ and OH^-.

the regular versions of PBE0 and TPSS0 exhibit a convex curvature behavior in both the electron removal and electron gain regions, which is quite common as traditional XC functionals of DFT are subjected to this test.

On the other hand, the COT variants (PBE0 IP, TPSS0 IP, PBE0 HL, and TPSS0 HL) more closely follow the exact line during the electron removal, while exhibiting now a concave curvature in the electron addition region.

However, a completely different behavior is observed for the variants of the LC-PBE0 functional investigated here. Now, the three versions closely follow a straight line in the electron removal region, although the LC-PBE0 IP seems to deviate more compared to the other two. This trend is also observed along the electron gain process; that is, while the regular LC-PBE0 and LC-PBE0 HL versions remain closer to the "exact" line, LC-PBE0 IP deviates more significantly and exhibits a concave curvature, similarly to the behavior seen with all the other functionals derived from the IP condition in this region.

The discussion regarding the convexity and concavity of the functionals is further clarified in Fig. 3. This figure illustrates the deviation from piecewise linearity for a fluorine atom with a fractional number of electrons, connecting the neutral species (number of electrons, N = 9) with its cationic (N = 8) and anionic (N = 10) forms. The plot shows how the total energies of the fractional electron systems deviate from the ideal piecewise linear interpolation defined by the energies of the integer electron systems. Notably, the functionals from the IP condition (PBE0 IP, TPSS0 IP, and LC-PBE0 IP) show excellent behaviors along the electron removal process, as evidenced by their deviation curves staying closer to zero throughout this interpolation range. This behavior indicates minimal localization/delocalization errors in comparison to the regular functionals for such an ionization process. Although global-hybrid functionals derived from the HL condition also show excellent improvement in the electron-loss region compared to the regular ones, their true strength emerges in the electron-gain process, as they closely follow the expected behavior. Similarly, LC-PBE0 HL achieves remarkable results along the electron gain region, while the original LC-PBE0 shows concave curvatures here, and the functionals obtained from the IP condition exhibit convex behavior along this process.

C. One-particle spectrum

We also evaluated the performance of all PBE-like functionals in predicting the one-particle spectrum by calculating vertical ionization potentials (IPs) from orbital eigenvalues, i.e., by comparing the reference IPs to the negative of the eigenvalues obtained for occupied orbitals. Table III presents the deviations of the functionals from the IP-EOM-CCSD/cc-pVTZ reference values.[21] The test set includes 401 valence ionization potentials from 63 molecules.

As is well known, the PBE0 functional does not provide accurate orbital eigenvalues, resulting in a poor description of such IPs. For example, the MAD of PBE0 across the entire set of valence IPs is 3.06 eV, with a MAX value of 8.45 eV. Reparameterization using the IP condition significantly improves the accuracy, reducing the MAD to 0.61 eV and the MAX to 3.02 eV. In addition, the PBE0 HL variant performs even better for the entire set, giving a MAD of 0.41 eV and a MAX of 3.61 eV. Moreover, the mean signed deviation (MSD) values indicate that the regular PBE0 (MSD = −3.03 eV) significantly underestimates the IPs, whereas PBE0 IP (MSD = 0.47 eV)

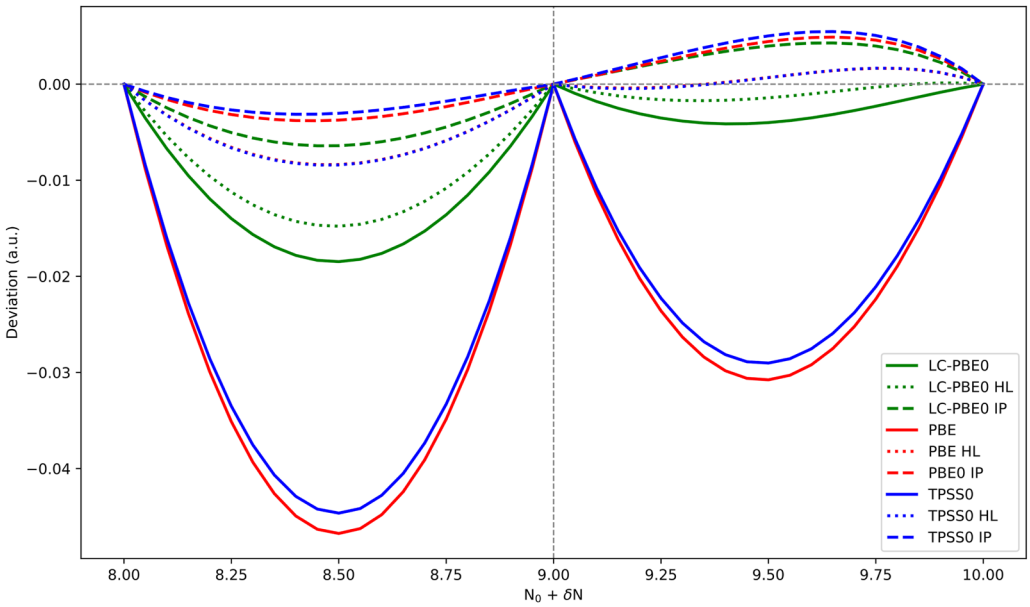

FIG. 3. Deviation of PBE-based functionals from the piecewise linear interpolation regarding the fractional electron occupancies.

TABLE III. Mean absolute deviation (MAD), mean signed deviation (MSD), and maximum absolute deviation (MAX) in vertical ionization potentials (eV) for the 401IP test set computed with PBE-like functionals relative to IP-EOM-CCSD reference values.[21] The basis set used is cc-pVTZ.[a]

	All valence			HOMO		
	MAD	MSD	MAX	MAD	MSD	MAX
PBE0	3.06	−3.03	8.45	2.95	−2.89	4.37
PBE0 IP	0.61	0.47	3.02	0.37	−0.11	0.97
PBE0 HL	0.41	0.08	3.61	0.49	−0.42	1.25
TPSS0	2.99	−2.99	8.14	2.89	−2.89	4.24
TPSS0 IP	0.65	0.47	4.66	0.37	−0.09	1.02
TPSS0 HL	0.41	0.05	3.59	0.51	−0.45	1.30
LC-PBE0	0.32	−0.03	4.85	0.29	−0.16	1.17
LC-PBE0 IP	0.59	0.52	3.44	0.29	0.11	0.79
LC-PBE0 HL	0.33	0.17	4.42	0.25	−0.03	0.83
QTP00	0.65	0.58	3.48	0.32	0.16	0.92
QTP01	0.31	−0.05	5.03	0.29	−0.16	1.14
QTP02	0.34	0.20	4.51	0.24	0.00	0.79

[a]Notes: "Regular" refers to the original functional; "IP" indicates that the parameterization obeys the ionization condition from COT; and "HL" indicates that the functional obeys the HOMO/LUMO conditions from COT. The results for the QTP functionals were retrieved from Ref. 21.

and the PBE0 HL (MSD = 0.08 eV) overestimate these values to a small extent.

Although the regular TPSS0 functional yields better results than the regular PBE0, the errors remain significant, with a MAD of 2.99 eV and a MAX of 8.14 eV. The previously observed trend persists under the different COT conditions: the IP and HL conditions improve the accuracy. However, when comparing the reparameterized versions of TPSS0 to those of PBE0, the latter performs better overall. For example, TPSS0 IP yields a MAD of 0.65 eV and a MAX of 4.66 eV, while TPSS0 HL exceptionally results in a MAD of 0.41 eV and a MAX of 3.59 eV. As before, the regular TPSS0 significantly underestimates the IPs, with an MSD of −2.99 eV. In contrast, TPSS0 IP and TPSS0 HL overestimate the values slightly, with MSDs of 0.47 and 0.05 eV, respectively.

Range separation appears to significantly correct the IP spectrum issues observed for the regular PBE0. For example, LC-PBE0 produces an MAD of 0.32 eV, compared to 0.59 eV for LC-PBE0 IP and 0.33 eV for LC-PBE0 HL. In this case, applying the COT conditions does not substantially alter the results. Again, the HOMO/LUMO condition performs better than the IP condition. Interestingly, the MAX value for regular LC-PBE0 is the largest among RSH functionals, at 4.85 eV, while LC-PBE0 IP and LC-PBE0 HL show MAX values of 3.44 and 4.42 eV, respectively. All LC-PBE0 variants yield small MSD values: the regular version slightly underestimates the IPs (−0.03 eV), while the IP and HL versions overestimate them, with MSDs of 0.52 and 0.17 eV, respectively.

In fact, the existing QTP functionals also provide very accurate results compared to IP-EOM-CCSD/cc-pVTZ considering the 401 IP set.[21] Therefore, QTP01, QTP02, and QTP00 provide MAD values of 0.31 eV, 0.34 eV, and 0.65 eV, respectively. This reinforces the excellent performance of all LC-PBE0 versions for this particular property.

Table III also presents data that focus exclusively on HOMO energies (i.e., the first ionization potentials). In this case, the performance ranks from the best to the worst as follows for global hybrids: IP condition, HOMO/LUMO condition, and regular. Therefore, the best performances among global hybrids are those from PBE0 IP (MAD = 0.37 eV) and TPSS0 IP (MAD = 0.37 eV). All PBE0

variants underestimate the results. Similarly, all TPSS0 versions underestimate the HOMO energies (to different extents), with TPSS0 IP achieving a nearly null MSD value. As seen before for the range-separated hybrids, all LC-PBE0 variants yield again quite small MAD values nearby 0.25–0.29 eV, with MSD values of −0.16 eV (for regular LC-PBE0), 0.11 eV (for LC-PBE0 IP), and −0.03 eV (for LC-PBE0 HL).

Next, our investigation is extended to vertical electron affinities (see Table IV). Therefore, starting with functionals derived from both PBE0 and TPSS0, the worst performance is achieved by the regular versions. For example, PBE0 and TPSS0 give MAD values of 1.41 and 1.30 eV, respectively. In contrast, the IP-based versions of these functionals perform better than their regular counterparts, i.e., PBE0 IP with a MAD of 0.23 eV and TPSS0 IP with a MAD of 0.21 eV. The HL forms closely follow in performance, as both PBE0 HL and TPSS0 HL achieve a MAD of 0.33 eV. Surprisingly, all forms of LC-PBE0 perform very well for this property, with MAD values ranging from 0.12 to 0.16 eV.

In addition, the majority of the XC functionals from Table IV overestimate the EA results. For example, for the global hybrids, the MSD ranges from 0.21 to 1.41 eV, respectively, for TPSS0 IP and regular PBE0. MSD concerning LC-PBE0 derivatives ranges from −0.01 to 0.01 eV, respectively, for LC-PBE0 IP and regular LC-PBE0. The maximum deviation values for all IP-based functionals are up to 0.54 eV (PBE0 IP), while HL-based have MAX up to 0.77 eV (PBE HL), and the regular versions are up to 2.77 eV (PBE0).

In this case, all the PBE-like functionals were unable to get even close to the great performance of the QTP functionals for the same test set. For instance, LC-QTP achieved the best result with a MAD of 0.08 eV, followed closely by QTP02 with a MAD of 0.11 eV. The third-best performance was obtained with QTP01 (MAD = 0.18 eV), followed by QTP00 (MAD = 0.20 eV). All relevant numerical results are provided in the supplementary material. However, it is important to mention that a far more detailed investigation of vertical electron affinity was conducted by Pavlicek and co-workers.[22]

D. Challenges: Charge-transfer and barrier heights

One common limitation of contemporary KS-TDDFT is the difficulty in accurately predicting excitation energies to charge-transfer (CT) states. In our study, we focus specifically on long-range charge-transfer (LR-CT) excitations, which are closely linked to the inability of existing XC functionals to correctly capture the integer discontinuity, often resulting in large underestimations of excitation energies.[55] To investigate this, we analyze the $NH_3\cdots HNO_2$ dimer at nine different intermolecular distances (d) from the LRCTEE9 test set.[56] All LR-CT information is shown in Table V.

The results obtained with the original versions of PBE0 and TPSS0 highlight the difficulty that standard XC functionals face in describing CT states. For example, the conventional PBE0 functional yields a MAD of 4.98 eV and a MAX of 5.65 eV relative to the reference data. A similar trend is observed for the MGGA functional TPSS0, with a MAD of 4.81 eV and a MAX of 5.49 eV. It is worth noting that, since analytic second derivatives are not implemented for MGGA functionals in NWChem, all TPSS0 linear response calculations were performed using Orca 6.0.1.[57]

In contrast, introducing range separation largely solves this issue. For instance, LC-PBE0 achieves a MAD of just 0.80 eV, representing an improvement of more than 4 eV over standard PBE0! The MAX value of LC-PBE0 is also significantly lower, 0.85 eV.

However, applying COT via the IP condition offers a much simpler and, perhaps, more effective solution to this issue, as seen when this approach is followed starting with PBE0; that is, PBE0 IP now provides a significantly reduced MAD of 0.75 eV. Although the MAX of PBE0 IP (1.01 eV) remains higher than that of LC-PBE0, this value is now much smaller than that from the standard PBE0. A similar improvement is observed for TPSS0. Hence, TPSS0 IP achieves a MAD of 0.70 eV and a MAX of 0.94 eV. These results suggest that both global hybrid functionals can become suitable alternatives for simulating such a challenging property as long-range charge transfer when corrected via the IP condition.

TABLE IV. Vertical electron affinity obtained using PBE-like functionals and mean absolute deviation (MAD) with respect to EA-EOM-CCSD results (eV).[22] The basis set used is aug-cc-pVTZ.[a]

		PBE0			TPSS0			LC-PBE0		
	EA-EOM-CCSD	Regular	IP	HL	Regular	IP	HL	Regular	IP	HL
NH_3	−0.62	0.21	−0.48	−0.42	0.13	−0.50	−0.43	−0.71	−0.71	−0.72
H_2O	−0.63	0.34	−0.44	−0.37	0.25	−0.46	−0.38	−0.68	−0.68	−0.69
H_2CO	−0.60	1.47	−0.49	−0.34	1.30	−0.49	−0.36	−0.69	−0.67	−0.69
N_2	−2.12	0.66	−1.57	−1.35	0.53	−1.61	−1.36	−1.72	−1.89	−1.79
CO	−1.59	0.81	−1.06	−0.90	0.68	−1.09	−0.90	−1.32	−1.38	−1.36
CO_2	−0.93	0.22	−0.76	−0.67	0.11	−0.79	−0.68	−1.07	−1.07	−1.08
C_2H_2	−0.71	−0.21	−0.64	−0.60	−0.25	−0.65	−0.60	−0.82	−0.81	−0.81
HCN	−0.52	0.06	−0.44	−0.40	−0.06	−0.45	−0.40	−0.61	−0.60	−0.61
MAD		1.41	0.23	0.33	1.30	0.21	0.33	0.16	0.12	0.14
MSD		1.41	0.23	0.33	1.30	0.21	0.33	0.01	−0.01	0.00
MAX		2.77	0.54	0.77	2.65	0.50	0.76	0.40	0.23	0.32

[a]Notes: "Regular" refers to the original functional; "IP" indicates the parameterization that obeys the ionization condition from COT; and "HL" indicates the functional that obeys the HOMO/LUMO conditions from COT.

TABLE V. Vertical excitation energies (eV) for long-range charge-transfer excited states of the NH_3···HNO_2 dimer obtained in TDDFT calculations with the jul-cc-pVTZ basis set and deviations with respect to reference results from Ref. 56.

		PBE0			TPSS0			LC-PBE0		
d(NH_3···HNO_2)	References[a]	Regular	IP	HL	Regular	IP	HL	Regular	IP	HL
3.6772	7.10	3.94	7.23	6.87	4.12	7.31	6.89	6.52	6.90	6.67
6.1133	8.22	3.90	7.77	7.35	4.06	7.84	7.34	7.45	7.73	7.59
8.5632	8.75	3.97	8.12	7.66	4.13	8.19	7.66	7.97	8.25	8.12
11.0156	9.13	4.03	8.34	7.86	4.19	8.41	7.85	8.29	8.57	8.43
13.4708	9.35	4.07	8.48	8.00	4.23[b]	8.56	7.99	8.51[b]	8.78	8.65
15.9272	9.51	4.10	8.59	8.10	4.27	8.66	8.08	8.66	8.93	8.80
18.3868	9.62	4.13	8.67	8.17	4.29	8.74	8.15	8.77	9.05	8.91
23.3034	9.77	4.17	8.78	8.27	4.33	8.85	8.25	8.93	9.20	9.07
25.7630	9.83	4.18	8.82	8.31	4.34	8.89	8.29	8.98	9.26	9.12
MAD		4.98	0.75	1.19	4.81	0.70	1.20	0.80	0.51	0.66
MSD		−4.98	−0.72	−1.19	−4.81	−0.65	−1.20	−0.80	−0.51	−0.66
MAX		5.65	1.01	1.52	5.49	0.94	1.54	0.85	0.58	0.71

[a]The reference data were obtained using MS-CASPT2.
[b]Values obtained using the Tamm–Dancoff approximation due to convergence issues at the full TDDFT level.

In addition, even greater accuracy is achieved when the IP condition is applied on top of LC-PBE0. The best performance in Table V is obtained with LC-PBE0 IP, which yields a MAD of 0.51 eV and a MAX of 0.58 eV.

Next, regarding the HOMO/LUMO condition, the global hybrid functionals derived from this approach performed better than their original counterparts and worse than the IP derivatives. For example, PBE0 HL and TPSS0 HL yield MAD values of 1.19 and 1.20 eV, respectively. Similarly, LC-PBE0 HL shows improved performance over its original version, with a MAD of 0.66 eV, providing the second-best overall results for LR-CT predictions.

Finally, the MSD results indicate that all forms of the XC functionals studied tend to underestimate the LR-CT excitation energies relative to the reference dataset, which is in accordance with Tozer.[55] The MSD values range from −4.98 eV for the original PBE0 to −0.51 eV for LC-PBE0 IP.

Mendes and co-workers[17] evaluated the performance of the QTP functionals for LR-CT under the same conditions used in this study. Their results showed that LC-QTP delivered the best performance, with a MAD of 0.16 eV. The remaining QTP functionals are ranked as follows: QTP00 (MAD = 0.37 eV), QTP02 (MAD = 0.42 eV), and QTP01 (MAD = 0.84 eV). These results indicate that, although COT enhances the performance of the PBE-based functionals, neither of the new variants nor the standard forms outperforms most of the QTP functionals.

For completeness, we also investigate an additional charge-transfer test set that includes ten different dimers: NH_3···F_2, C_3H_6O···F_2, $C_4H_4N_2$···F_2, C_3H_6O···CH_3NO_2, C_4H_5N···$C_4H_4N_2$ (H-bonded), C_4H_5N···$C_4H_4N_2$ (stacked), C_2F_4···C_2H_4 (d = 5 Å), C_2F_4···C_2H_4 (d = 3.5 Å), NH_3···OF_2, and NH_3···$C_4H_4N_2$. The geometries and reference values were obtained from Kozma *et al.*[58] Absolute and signed deviations are shown in Fig. 4, while maximum deviations and raw data are presented in Table S4.

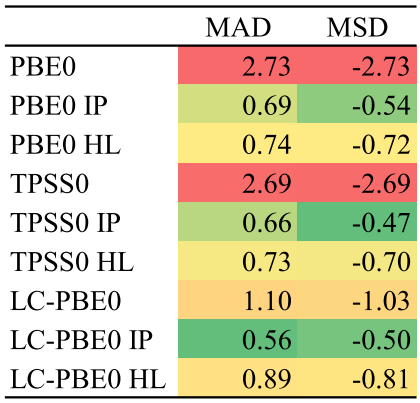

FIG. 4. Heat map showing the mean absolute deviation (MAD) and mean signed deviation (MSD), in eV, of the calculated charge-transfer excited states with respect to EOM-CCSDT-3 reference data from Kozma *et al.*[58] The cc-pVDZ basis set was used.

In another study,[51] charge transfer was reported for a set of TCNE molecules, exhibiting a linear behavior on the distance between two units based on six data points.

As observed previously, enforcing both COT conditions substantially improves the performance of all functionals for charge transfer, e.g., reducing the MAD by more than 2 eV in the case of global hybrids modified by the IP condition. Once again, both conditions contribute positively to the RSH LC-PBE0 functional. In this test, the best performance is achieved by LC-PBE0 IP, with a MAD of 0.56 eV. TPSS0 IP and PBE0 IP rank second and third, respectively. Within the same methodology, the QTP functionals perform as follows:[17] QTP00 yields a MAD of 0.36 eV, QTP02 gives 0.61 eV, LC-QTP results in 0.69 eV, and QTP01 presents a MAD of 0.76 eV.

As the final test of KS-DFT performance for challenging properties, the ability of PBE-like functionals in reproducing the reaction barrier heights of the BH76 test set is evaluated. This test set is a combination of the NHTBH38 and HTBH38 databases from Verma and coworkers[56] and considers forward and reverse reaction directions. The MADs for these systems are presented in Fig. 5, and the MSD values are illustrated in Fig. 6. The actual barrier height and MAX values are provided in Table S5 in the supplementary material.

Therefore, the comparison of the regular, IP, and HL variants of the three hybrid functionals studied herein, PBE0, TPSS0, and LC-PBE0, reveals some differences related to the barrier height accuracy. For example, PBE0 yields a MAD of 3.99 kcal/mol, which is not improved with IP condition (4.03 kcal/mol). However, under the HOMO/LUMO condition, PBE0 achieves its best performance, MAD = 3.51 kcal/mol. The maximum error goes from 14.17 kcal/mol (PBE0) to 12.77 kcal/mol (PBE0 IP), while

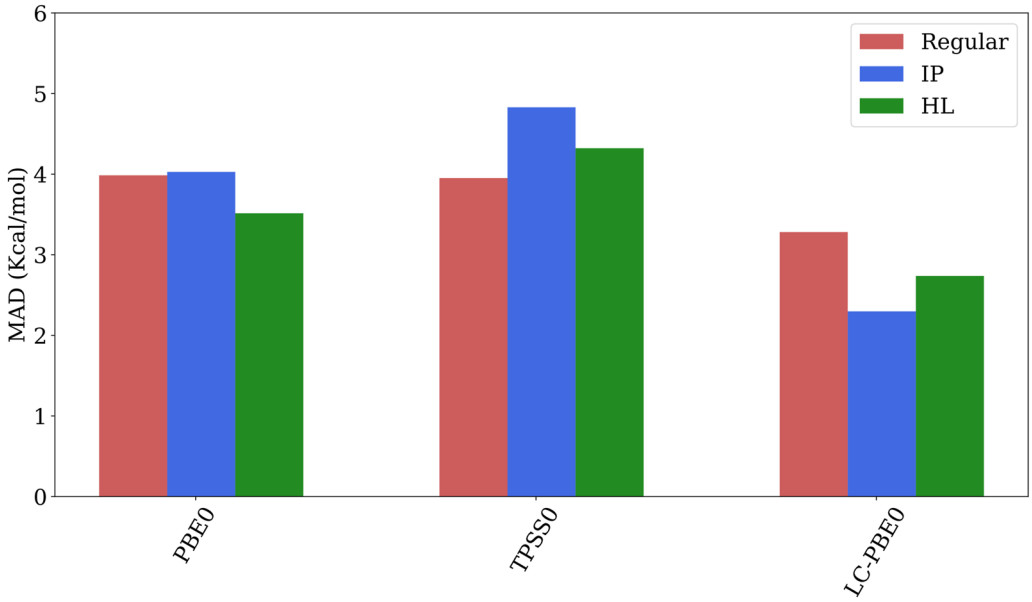

FIG. 5. Mean absolute deviations (MADs) obtained using PBE-like exchange-correlation functionals compared to the reference values from Verma *et al.*[56] (in kcal/mol). The basis set used is def2-QZVP.

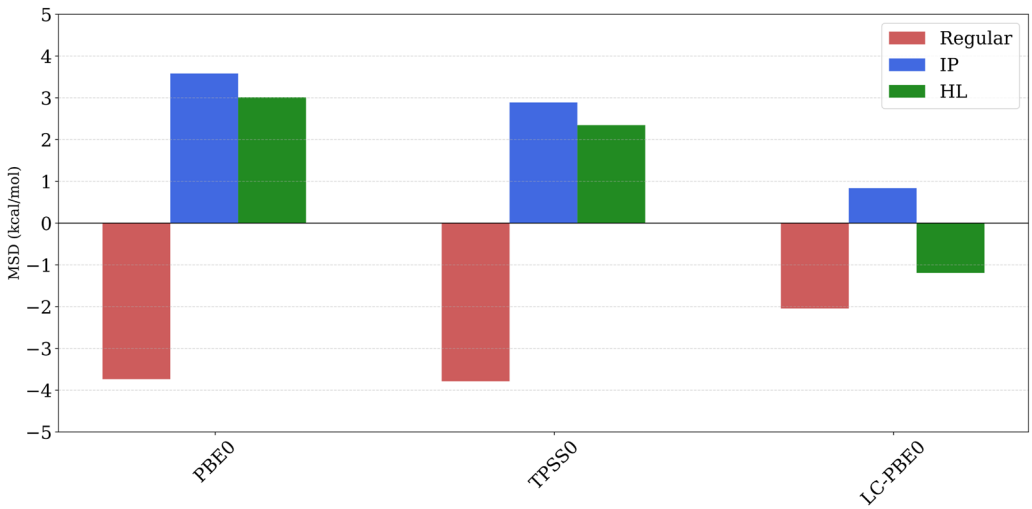

FIG. 6. Mean signed deviations (MSDs) obtained using PBE-like exchange-correlation functionals compared to the reference values from Verma *et al.*[56] (in kcal/mol). The basis set used is def2-QZVP.

the MSD varies from −3.74 kcal/mol (PBE0) to 3.58 kcal/mol (PBE0 IP).

In contrast, the original TPSS0 exhibits better performance compared to its COT variants, i.e., MAD = 3.95 kcal/mol. The MAD from TPSS0 IP is 4.83 kcal/mol, and the one from TPSS0 HL is 4.32 kcal/mol. The MSD values also reflect consistent trends observed previously: −3.79 kcal/mol for the regular version, 2.89 kcal/mol for the IP one, and 2.35 kcal/mol for TPSS0 HL. Notably, the IP condition version of TPSS0 presents the largest MAX value among all TPSS0 variants (16.48 kcal/mol).

The three best-ranked functionals in this analysis come from all LC-PBE0 variants. Furthermore, in this case, both COT strategies yield improvements over the regular version. The MAD decreases from 3.28 kcal/mol (regular) to 2.30 kcal/mol (IP condition) and 2.74 kcal/mol (HL condition). Similarly, the MAX errors are lower in the COT variants, with the LC-PBE0 HL showing the smallest overall maximum deviation (8.77 kcal/mol). The MSD values reveal reduced systematic errors upon COT reparameterization: from −2.04 kcal/mol (regular) to 0.84 kcal/mol (LC-PBE0 IP) and −1.19 kcal/mol (LC-PBE0 HL), supporting the benefits of applying COT to obtain the optimum amount of HF exchange, particularly by means of the IP condition.

V. CONCLUSIONS

We investigated the potential improvements of three hybrid functionals from the PBE family by applying the conditions established by the correlated orbital theory. To this end, we selected PBE-like hybrid XC functionals from different rungs of Jacob's ladder: PBE0 (GGA), TPSS0 (MGGA), and LC-PBE0 (RSH). Two reparameterization strategies were employed to optimize the admixture of HF and PBE-like exchange: (*i*) the IP condition and (*ii*) the HOMO/LUMO condition.

Reparameterization based on the IP condition favored significantly larger fractions of HF exchange into the new functionals compared to their original versions (25%), reaching 71% in PBE0 IP and TPSS0 IP. In comparison, the HOMO/LUMO condition led to slightly smaller HF exchange fractions (although still large), yielding 66% for PBE0 HL and 65% for TPSS0 HL. In the case of LC-PBE0, we also enforced the condition $\alpha + \beta = 1$, ensuring that all variants contain 100% of HF exchange in the long-range limit. However, the amount of HF exchange in the short-range was increased under both reparameterization strategies: the IP condition led to 57% HF exchange, while the HOMO/LUMO condition resulted in 34%.

Next, regarding the self-interaction error, which is clearly present in the original (regular) versions of PBE0 and TPSS0, as evidenced by their inaccurate reproduction of the H_2^+ potential energy curve, the enforcement of the IP and HOMO/LUMO conditions from COT significantly mitigates this issue in both functionals. Although all variants of LC-PBE0 demonstrate nice energy results for the H_2^+ energy curve, both the IP and HOMO/LUMO versions perform slightly better than the original form of such a functional in this respect.

The next step was to investigate how well the functionals reproduce the energy profile of a system as electrons are added or removed. Deviations from straight-line behavior in this context are referred to as manifestations of integer discontinuity issues. First, considering PBE0 and TPSS0, in general, both COT versions more closely follow the exact, piecewise-linear behavior expected from the exact theory. However, the IP variants perform better in the "electron removal" region, while the HL condition guarantees better behavior in the "electron addition" region. In contrast, the LC-PBE0 variants exhibit a distinct pattern: all three versions perform well considering the expected straight line in the electron removal region, and there are some signs of improvement caused by COT in this aspect. However, in the electron addition region, the LC-PBE0 IP version shows a significant deviation in the opposite direction to the one observed with the original version of this functional, while the HOMO/LUMO variant more closely follows the expected linear behavior.

Analyzing the one-particle spectra, both COT variants of PBE0 and TPSS0 largely outperform their original versions. In this case, the HL-optimized global hybrids showed the best performances. Once again, considering the entire 401 valence IPs, all variants of LC-PBE0 demonstrate excellent performance. An additional investigation considered the first electron affinities for a smaller test set. This study revealed, not surprisingly, that the IP and HL optimized versions of PBE0 and TPSS0 yield excellent results compared to the original functionals. At the same time, all LC-PBE0 functionals performed very well.

One of the major challenges faced by KS DFT is the accurate description of charge-transfer processes, particularly at long range, since this difficulty is closely tied to the correct treatment of the derivative discontinuity issue. Therefore, to illustrate the impact of COT on this, we considered the $NH_3\cdots HNO_2$ dimer set, where the use of the IP condition demonstrated its effectiveness. Specifically, it reduces the error seen in standard PBE-like global hybrids from as much as 4.81–4.98 eV to as little as 0.70–0.75 eV. Next, both COT conditions also improve the already nice performance of LC-PBE0. For a second CT test set, composed of ten dimers and 13 states, the performance pattern is exactly the same.

Accurate prediction of reaction barrier heights remains a significant challenge. In this case, the best results are obtained for all LC-PBE0 variants, with the IP condition yielding the lowest deviations, closely followed by the HL version. On the other hand, applying the COT conditions on top of TPSS0 for the BH76 test set actually worsens the accuracy compared to the original functional. In contrast, the HOMO/LUMO condition improves the performance of PBE0.

Overall, we demonstrated that enforcing the principles of correlated orbital theory in hybrid functionals from the PBE family appears to yield benefits along various rungs of Jacob's ladder of exchange-correlation functionals. However, none offer improvements over the QTP family of functionals for the examples studied.

SUPPLEMENTARY MATERIAL

All numerical results obtained during the conception of this study are reported within the supplementary material.

ACKNOWLEDGMENTS

This study was supported by the Air Force Office of Scientific Research under AFOSR Award No. FA9550-23-1-0118. R.L.A. Haiduke also acknowledges the National Council for Scientific and

Technological Development (CNPq–Grant No. 306763/2021-4) for financial support.

AUTHOR DECLARATIONS

Conflict of Interest

The authors have no conflicts to disclose.

Author Contributions

Rodrigo A. Mendes: Conceptualization (equal); Data curation (equal); Formal analysis (equal); Investigation (equal); Methodology (equal); Writing – original draft (equal). **Zachary W. Windom**: Conceptualization (equal); Investigation (supporting); Methodology (equal); Writing – review & editing (equal). **Roberto L. A. Haiduke**: Conceptualization (equal); Formal analysis (equal); Methodology (equal); Project administration (equal); Writing – review & editing (equal). **Rodney J. Bartlett**: Conceptualization (equal); Funding acquisition (equal); Methodology (equal); Project administration (equal); Resources (equal); Writing – review & editing (equal).

DATA AVAILABILITY

The data that support the findings of this study are available within the article and its supplementary material.

REFERENCES

[1]P. Hohenberg and W. Kohn, "Inhomogeneous electron gas," Phys. Rev. **136**, B864–B871 (1964).
[2]W. Kohn and L. J. Sham, "Self-consistent equations including exchange and correlation effects," Phys. Rev. **140**, A1133–A1138 (1965).
[3]J. P. Perdew, K. Burke, and M. Ernzerhof, "Generalized gradient approximation made simple," Phys. Rev. Lett. **77**, 3865–3868 (1996).
[4]J. P. Perdew and K. Schmidt, "Jacob's ladder of density functional approximations for the exchange-correlation energy," AIP Conf. Proc. **577**, 1–20 (2001).
[5]J. P. Perdew, S. Kurth, A. Zupan, and P. Blaha, "Accurate density functional with correct formal properties: A step beyond the generalized gradient approximation," Phys. Rev. Lett. **82**, 2544–2547 (1999).
[6]J. Tao, J. P. Perdew, V. N. Staroverov, and G. E. Scuseria, "Climbing the density functional ladder: Nonempirical meta–generalized gradient approximation designed for molecules and solids," Phys. Rev. Lett. **91**, 146401 (2003).
[7]T. Leininger, H. Stoll, H.-J. Werner, and A. Savin, "Combining long-range configuration interaction with short-range density functionals," Chem. Phys. Lett. **275**, 151–160 (1997).
[8]R. D. Adamson, J. P. Dombroski, and P. M. W. Gill, "Efficient calculation of short-range Coulomb energies," J. Comput. Chem. **20**, 921–927 (1999).
[9]H. Iikura, T. Tsuneda, T. Yanai, and K. Hirao, "A long-range correction scheme for generalized-gradient-approximation exchange functionals," J. Chem. Phys. **115**, 3540–3544 (2001).
[10]M. A. Rohrdanz and J. M. Herbert, "Simultaneous benchmarking of ground- and excited-state properties with long-range-corrected density functional theory," J. Chem. Phys. **129**, 034107 (2008).
[11]C. Adamo and V. Barone, "Toward reliable density functional methods without adjustable parameters: The PBE0 model," J. Chem. Phys. **110**, 6158–6170 (1999).
[12]O. A. Vydrov and G. E. Scuseria, "Assessment of a long-range corrected hybrid functional," J. Chem. Phys. **125**, 234109 (2006).
[13]M. A. Rohrdanz, K. M. Martins, and J. M. Herbert, "A long-range-corrected density functional that performs well for both ground-state properties and time-dependent density functional theory excitation energies, including charge-transfer excited states," J. Chem. Phys. **130**, 054112 (2009).
[14]W. Chen, G. Miceli, G.-M. Rignanese, and A. Pasquarello, "Nonempirical dielectric-dependent hybrid functional with range separation for semiconductors and insulators," Phys. Rev. Mater. **2**, 073803 (2018).
[15]B. Moore II, A. Charaf-Eddin, A. Planchat, C. Adamo, J. Autschbach, and D. Jacquemin, "Electronic band shapes calculated with optimally tuned range-separated hybrid functionals," J. Chem. Theory Comput. **10**, 4599–4608 (2014).
[16]J. W. Knight, X. Wang, L. Gallandi, O. Dolgounitcheva, X. Ren, J. V. Ortiz, P. Rinke, T. Körzdörfer, and N. Marom, "Accurate ionization potentials and electron affinities of acceptor molecules III: A benchmark of GW methods," J. Chem. Theory Comput. **12**, 615–626 (2016).
[17]R. A. Mendes, R. L. A. Haiduke, and R. J. Bartlett, "The Devil's triangle of Kohn–Sham density functional theory and excited states," J. Chem. Phys. **154**, 074106 (2021).
[18]J. L. Bao, L. Gagliardi, and D. G. Truhlar, "Self-interaction error in density functional theory: An appraisal," J. Phys. Chem. Lett. **9**, 2353–2358 (2018).
[19]D. S. Ranasinghe, J. T. Margraf, Y. Jin, and R. J. Bartlett, "Does the ionization potential condition employed in QTP functionals mitigate the self-interaction error?," J. Chem. Phys. **146**, 034102 (2017).
[20]P. Mori-Sánchez and A. J. Cohen, "The derivative discontinuity of the exchange-correlation functional," Phys. Chem. Chem. Phys. **16**, 14378–14387 (2014).
[21]D. S. Ranasinghe, J. T. Margraf, A. Perera, and R. J. Bartlett, "Vertical valence ionization potential benchmarks from equation-of-motion coupled cluster theory and QTP functionals," J. Chem. Phys. **150**, 074108 (2019).
[22]A. Pavlicek, Z. W. Windom, A. Perera, and R. J. Bartlett, "A comparison of QTP functionals against coupled-cluster methods for EAs of small organic molecules," J. Chem. Phys. **160**, 014106 (2024).
[23]R. J. Bartlett, "Towards an exact correlated orbital theory for electrons," Chem. Phys. Lett. **484**, 1–9 (2009).
[24]J. P. Perdew and A. Zunger, "Self-interaction correction to density-functional approximations for many-electron systems," Phys. Rev. B **23**, 5048–5079 (1981).
[25]C. Li, X. Zheng, A. J. Cohen, P. Mori-Sánchez, and W. Yang, "Local scaling correction for reducing delocalization error in density functional approximations," Phys. Rev. Lett. **114**, 053001 (2015).
[26]M. R. Pederson, A. Ruzsinszky, and J. P. Perdew, "Communication: Self-interaction correction with unitary invariance in density functional theory," J. Chem. Phys. **140**, 121103 (2014).
[27]P. Verma and R. J. Bartlett, "Increasing the applicability of density functional theory. IV. Consequences of ionization-potential improved exchange-correlation potentials," J. Chem. Phys. **140**, 18A534 (2014).
[28]Y. Jin and R. J. Bartlett, "The QTP family of consistent functionals and potentials in Kohn–Sham density functional theory," J. Chem. Phys. **145**, 034107 (2016).
[29]R. L. A. Haiduke and R. J. Bartlett, "Non-empirical exchange-correlation parameterizations based on exact conditions from correlated orbital theory," J. Chem. Phys. **148**, 184106 (2018).
[30]T. Yanai, D. P. Tew, and N. C. Handy, "A new hybrid exchange–correlation functional using the Coulomb-attenuating method (CAM-B3LYP)," Chem. Phys. Lett. **393**, 51–57 (2004).
[31]Y. Jin and R. J. Bartlett, "Accurate computation of x-ray absorption spectra with ionization potential optimized global hybrid functional," J. Chem. Phys. **149**, 064111 (2018).
[32]A. D. Becke, "Density-functional exchange-energy approximation with correct asymptotic behavior," Phys. Rev. A **38**, 3098–3100 (1988).
[33]A. D. Becke, "Density-functional thermochemistry. III. The role of exact exchange," J. Chem. Phys. **98**, 5648–5652 (1993).
[34]C. Lee, W. Yang, and R. G. Parr, "Development of the Colle–Salvetti correlation-energy formula into a functional of the electron density," Phys. Rev. B **37**, 785–789 (1988).
[35]P. J. Stephens, F. J. Devlin, C. F. Chabalowski, and M. J. Frisch, "Ab initio calculation of vibrational absorption and circular dichroism spectra using density functional force fields," J. Phys. Chem. **98**, 11623–11627 (1994).

[36]R. A. Mendes, N. J. King, A. Brown, R. J. Bartlett, and M. Klobukowski, "cQTP25: A new exchange–correlation functional for core-electron ionization energy," J. Chem. Phys. **163**, 184107 (2025).
[37]Z. W. Windom, A. Perera, and R. J. Bartlett, "Benchmarking isotropic hyperfine coupling constants using (QTP) DFT functionals and coupled cluster theory," J. Chem. Phys. **156**, 094107 (2022).
[38]Y. C. Park, A. Perera, and R. J. Bartlett, "Density functionals for core excitations," J. Chem. Phys. **157**, 094107 (2022).
[39]I. A. Elayan, L. Rib, R. A. Mendes, and A. Brown, "Beyond explored functionals: A computational journey of two-photon absorption," J. Chem. Theory Comput. **20**, 3879–3893 (2024).
[40]R. A. Mendes, Z. W. Windom, H. Kim, and R. J. Bartlett, "On the performance of QTP functionals applied to second-order response properties," J. Chem. Phys. **162**, 054105 (2025).
[41]Z. W. Windom, A. Perera, and R. J. Bartlett, "Examining fundamental and excitation gaps at the thermodynamic limit: A combined (QTP) DFT and coupled cluster study on trans-polyacetylene and polyacene," J. Chem. Phys. **156**, 204308 (2022).
[42]E. Schwegler and M. Challacombe, "Linear scaling computation of the Hartree–Fock exchange matrix," J. Chem. Phys. **105**, 2726–2734 (1996).
[43]L. Meissner and R. J. Bartlett, "Electron propagator theory with the ground state correlated by the coupled-cluster method," Int. J. Quantum Chem. **48**, 67–80 (1993).
[44]M. Nooijen and J. G. Snijders, "Coupled cluster approach to the single-particle Green's function," Int. J. Quantum Chem. **44**, 55–83 (1992).
[45]M. Nooijen and J. G. Snijders, "Coupled cluster Green's function method: Working equations and applications," Int. J. Quantum Chem. **48**, 15–48 (1993).
[46]E. Aprà, E. J. Bylaska, W. A. de Jong, N. Govind, K. Kowalski, T. P. Straatsma, M. Valiev, H. J. J. van Dam, Y. Alexeev, J. Anchell, V. Anisimov, F. W. Aquino, R. Atta-Fynn, J. Autschbach, N. P. Bauman, J. C. Becca, D. E. Bernholdt, K. Bhaskaran-Nair, S. Bogatko, P. Borowski, J. Boschen, J. Brabec, A. Bruner, E. Cauët, Y. Chen, G. N. Chuev, C. J. Cramer, J. Daily, M. J. O. Deegan, T. H. Dunning, Jr., M. Dupuis, K. G. Dyall, G. I. Fann, S. A. Fischer, A. Fonari, H. Früchtl, L. Gagliardi, H. Früchtl, N. Gawande, S. Ghosh, K. Glaesemann, A. W. Götz, J. Hammond, A. W. Götz, E. D. Hermes, K. Hirao, S. Hirata, M. Jacquelin, L. Jensen, B. G. Johnson, H. Jónsson, R. A. Kendall, H. Jónsson, R. Kobayashi, V. Konkov, S. Krishnamoorthy, M. Krishnan, Z. Lin, R. D. Lins, R. J. Littlefield, A. J. Logsdail, K. Lopata, W. Ma, A. V. Marenich, J. Martin del Campo, D. Mejia-Rodriguez, J. E. Moore, J. M. Mullin, T. Nakajima, D. R. Nascimento, J. A. Nichols, P. J. Nichols, J. Nieplocha, A. Otero-de-la-Roza, B. Palmer, A. Panyala, T. Pirojsirikul, B. Peng, R. Peverati, J. Pittner, L. Pollack, R. M. Richard, P. Sadayappan, G. C. Schatz, W. A. Shelton, D. W. Silverstein, D. M. A. Smith, T. A. Soares, D. Song, M. Swart, H. L. Taylor, G. S. Thomas, V. Tipparaju, D. G. Truhlar, K. Tsemekhman, T. Van Voorhis, Á. Vázquez-Mayagoitia, P. Verma, A. Vázquez-Mayagoitia, A. Vishnu, K. D. Vogiatzis, D. Wang, J. H. Weare, M. J. Williamson, T. L. Windus, K. Woliński, A. T. Wong, K. Woliński, C. Yang, Q. Yu, M. Zacharias, Z. Zhang, Y. Zhao, R. J. Harrison, Y. Zhao, and R. J. Harrison, "NWChem: Past, present, and future," J. Chem. Phys. **152**, 184102 (2020).
[47]T. H. Dunning, Jr. and H. Thom, "Gaussian basis sets for use in correlated molecular calculations. I. The atoms boron through neon and hydrogen," J. Chem. Phys. **90**, 1007–1023 (1989).
[48]R. A. Kendall, T. H. Dunning, Jr., R. J. Harrison, and R. J. Harrison, "Electron affinities of the first-row atoms revisited. Systematic basis sets and wave functions," J. Chem. Phys. **96**, 6796–6806 (1992).
[49]E. Papajak and D. G. Truhlar, "Convergent partially augmented basis sets for post-Hartree–Fock calculations of molecular properties and reaction barrier heights," J. Chemical Theory Comput. **7**, 10–18 (2011).
[50]F. Weigend, F. Furche, and R. Ahlrichs, "Gaussian basis sets of quadruple zeta valence quality for atoms H–Kr," J. Chem. Phys. **119**, 12753–12762 (2003).
[51]R. J. Bartlett and D. S. Ranasinghe, "The power of exact conditions in electronic structure theory," Chem. Phys. Lett. **669**, 54–70 (2017).
[52]V. N. Staroverov, G. E. Scuseria, J. Tao, and J. P. Perdew, "Comparative assessment of a new nonempirical density functional: Molecules and hydrogen-bonded complexes," J. Chem. Phys. **119**, 12129–12137 (2003).
[53]J. P. Perdew, R. G. Parr, M. Levy, and J. L. Balduz, "Density-functional theory for fractional particle number: Derivative discontinuities of the energy," Phys. Rev. Lett. **49**, 1691–1694 (1982).
[54]A. J. Cohen, P. Mori-Sánchez, and W. Yang, "Development of exchange-correlation functionals with minimal many-electron self-interaction error," J. Chem. Phys. **126**, 191109 (2007).
[55]D. J. Tozer, "Relationship between long-range charge-transfer excitation energy error and integer discontinuity in Kohn–Sham theory," J. Chem. Phys. **119**, 12697–12699 (2003).
[56]P. Verma, Y. Wang, S. Ghosh, X. He, and D. G. Truhlar, "Revised M11 exchange-correlation functional for electronic excitation energies and ground-state properties," J. Phys. Chem. A **123**, 2966–2990 (2019).
[57]F. Neese, "Software update: The orca program system—Version 6.0," WIREs Comput. Mol. Sci. **15**, e70019 (2025) CMS-1186.R1.
[58]B. Kozma, A. Tajti, B. Demoulin, R. Izsák, M. Nooijen, and P. G. Szalay, "A new benchmark set for excitation energy of charge transfer states: Systematic investigation of coupled cluster type methods," J. Chem. Theory Comput. **16**, 4213–4225 (2020).